Aerospace Science and Technology 46 (2015) 436–450

Contents lists available at ScienceDirect

Aerospace Science and Technology

www.elsevier.com/locate/aescte

Radar/electro-optical data fusion for non-cooperative UAS sense and avoid

Giancarmine Fasano [a,*], Domenico Accardo [a], Anna Elena Tirri [a], Antonio Moccia [a], Ettore De Lellis [b]

[a] Department of Industrial Engineering – Aerospace Engineering Division, University of Naples "Federico II", P.le Tecchio 80, 80125 Napoli, Italy
[b] On-Board Systems and ATM Information Technologies Department, Italian Aerospace Research Center, Via Maiorise, 81043 Capua CE, Italy

ARTICLE INFO

Article history:
Received 4 July 2014
Received in revised form 30 June 2015
Accepted 10 August 2015
Available online 28 August 2015

Keywords:
Unmanned aircraft systems
Non-cooperative sense and avoid
Flight tests
Multi-sensor detection and tracking
Radar/electro-optical data fusion
Situational awareness

ABSTRACT

This paper focuses on hardware/software implementation and flight results relevant to a multi-sensor obstacle detection and tracking system based on radar/electro-optical (EO) data fusion. The sensing system was installed onboard an optionally piloted very light aircraft (VLA). Test flights with a single intruder plane of the same class were carried out to evaluate the level of achievable situational awareness and the capability to support autonomous collision avoidance. System architecture is presented and special emphasis is given to adopted solutions regarding real time integration of sensors and navigation measurements and high accuracy estimation of sensors alignment. On the basis of Global Positioning System (GPS) navigation data gathered simultaneously with multi-sensor tracking flight experiments, potential of radar/EO fusion is compared with standalone radar tracking. Flight results demonstrate a significant improvement of collision detection performance, mostly due to the change in angular rate estimation accuracy, and confirm data fusion effectiveness for facing EO detection issues. Relative sensors alignment, performance of the navigation unit, and cross-sensor cueing are found to be key factors to fully exploit the potential of multi-sensor architectures.

1. Introduction

Safe and efficient integration of Unmanned Aircraft Systems (UAS) into Civil Airspace is a key challenge for unleashing their potential for non-military applications [1] "without reducing existing capacity, decreasing safety, impacting current operators, or placing other airspace users or persons and property on the ground at increased risk" [2]. Integration challenges comprise airworthiness and certification, vulnerabilities of command and control link, human factors such as crew qualifications and training, air traffic management integration, and the lack of a see-and-avoid capability similar to manned aircraft. Considering sense and avoid, aeronautical agencies are currently working to detail the significance of general guidelines such as "equivalent levels of safety must be guaranteed with respect to manned aircraft" [3–5]. Following [6], in general sense and avoid consists of two components, such as separation assurance and collision avoidance. The first function reduces the probability of a collision by ensuring that the aircraft remain "well clear" of each other thereby assuring safe separation, while collision avoidance is related to extreme maneuvers just prior to closest point of approach to prevent collisions in cases where safe separation is lost.

While ground-based sense and avoid is a near term solution for meeting requirements thus enabling integration in limited operational areas [2,7], airborne surveillance for separation assurance and collision avoidance is the definite key asset to be accomplished and can be performed by two fundamental methods: cooperative instruments, wherein an aircraft is equipped with a transponder to interrogate and/or broadcast information, and non-cooperative sensors, which are able to detect targets autonomously. Automatic Dependent Surveillance Broadcast (ADS-B) and Traffic Alert and Collision Avoidance (TCAS) systems are classified as cooperative systems. In particular, the former is expected to play a key role for UAS integration also in the case of small UAS with limited budgets, becoming the primary safety system of autonomous, i.e., not dependent on command and control link, or remote pilot-based cooperative sense and avoid architectures [6,8,9].

Compared with ADS-B based solutions, non-cooperative architectures have the great advantage of guaranteeing detection and avoidance of non-equipped aircraft, and in the case of air-to-air radio link loss. However, they represent the most challenging case

* Corresponding author. Tel.: +39 0817682361; fax: +39 0817682160.
E-mail addresses: giancarmine.fasano@unina.it (G. Fasano), domenico.accardo@unina.it (D. Accardo), annaelena.tirri@unina.it (A.E. Tirri), antonio.moccia@unina.it (A. Moccia), e.delellis@cira.it (E. De Lellis).

http://dx.doi.org/10.1016/j.ast.2015.08.010

from the technological point of view, and fully certified sensing solutions seem to be achievable in a mid/far term perspective [2]. Nevertheless, a significant research effort is carried out worldwide to bridge the gap between existing technology and users requirements. Non-cooperative sensing systems are mainly studied in view of the collision avoidance function, and the proposed solutions range from standalone electro-optical (EO) sensors [10–13] to multi-sensor radar/EO systems [14]. Also, integrated architectures comprising radars, optical sensors, and cooperative systems, have been developed and tested in flight [15]. Recent efforts have been aimed at the development of autonomous collision avoidance architectures and algorithms [14–17] and of new radar sensors explicitly tailored for UAS collision avoidance [18,19].

Within the research project named TECVOL, the Italian Aerospace Research Center (CIRA) and the University of Naples developed an autonomous non-cooperative sense and avoid system which relies on an integrated radar/electro-optical (EO) configuration [14]. The prototype hardware/software system has been installed for flight demonstration onboard an optionally piloted laboratory aircraft of ultra light category named FLARE (Flying Laboratory for Aeronautical REsearch), which is a customized TECNAM P-92, and a flight test campaign has been carried out with a similar aircraft acting as intruder.

This work follows previous papers on radar-based detection and tracking [20], EO-based obstacle detection within the integrated sensor system [21], and autonomous non-cooperative collision avoidance experiments [22] and its focus is on radar/EO data fusion logics, algorithms, and flight results relevant to the achievable situational awareness. The paper is organized as follows. First of all, a general discussion is presented about potential benefits in adopting a multi-sensor approach for the sense and avoid problem. Then, after an overview of system architecture, developed algorithms are described in detail regarding real time multi-sensor tracking and relative sensors alignment. Finally, a thorough analysis of flight results relevant to near collision conditions is presented. Multi-sensor fusion output is analyzed and compared with standalone radar tracking especially focusing on the impact of tracking accuracy on collision detection reliability. On the basis of this comparison, general lessons learned, and considerations on data fusion role in the development of future collision avoidance systems, are provided.

2. Data fusion for sense and avoid

At a qualitative level [20], a non-cooperative sensing system for sense and avoid has to fulfill different requirements to guarantee an adequate level of safety, such as:

- detection range, that has to allow collision avoidance maneuvers to be completed keeping a minimum separation from intruders;
- angular field of regard, that also impacts obstacle tracking performance during avoidance maneuvers;
- uncertainty in estimating obstacle relative position and velocity, that directly affects collision detection performance in terms of false alarm rates and missed detection rates;
- measurement rates and latencies, that have to be adequate to provide confirmed detections in a reasonable time, and to track relative dynamics in case of maneuvers too, at least within certain limits.

Within this framework, the great potential for sense and avoid of multi-sensor architectures and real time fusion of measurements from heterogeneous sources, derives from the fact that different sensors have complementary features in view of the application. In fact, airborne radars provide direct and typically accurate range estimates, and also range rate if Doppler processing is used. Moreover, they can guarantee large detection range, low levels of missed or false detections (ground echoes have to be properly filtered, especially when flying at low altitude [20]), and are not much affected by weather conditions (indeed, this depends on the operating frequency [23]). However, standalone radar architectures are typically characterized by coarse angular resolutions and low update rates, since finer resolution essentially implies larger antenna dimensions, though coherent processing may be employed to improve this aspect [18] and electronic scanning allows increasing measurement rate in the case of confirmed tracks [18,19]. In general radars are demanding in terms of cost, size, weight and required electric power, so that they do not represent an affordable sensing solution for small unmanned platforms.

On the other hand, EO sensors offer the potential of highly accurate angular measurements at fast update rates and with limited budgets in terms of mass, power, size and cost. Coverage of a wide field of view can be guaranteed by installing multiple camera systems [10,13]. In general, EO systems require heavy computational resources in order to fulfill real-time full image detection of obstacles, and their output can suffer from a high false alarm rate. Obviously, optical image arrays are not capable to directly estimate range and range rate to obstacle, hence interest for low power range measuring sensors, such as laser rangefinders, arises [24,25]. In theory, multitemporal strategies based on scale change between consecutive images or ownship maneuvers [26] can allow estimating time to collision or range and range rate, but inadequate estimation accuracy, short time to collision, and aircraft maneuverability can limit the applicability of these approaches. More importantly, EO detection range and reliability can be very much affected by illumination and weather conditions, and can be poor.

On the basis of these considerations, it follows that integrated radar/EO systems can be a good sensing option to guarantee the required situational awareness in the case of medium/large UAS platforms, provided that real time data fusion is properly carried out. In general, the high level objective of the data fusion system is to integrate the best features of the dissimilar sensors while ensuring solution reliability and limiting the computational burden so enabling real time software implementation.

3. Architecture and algorithms

Within project TECVOL, a multi-sensor configuration has been selected which comprises an airborne Ka-band pulsed radar, two Infra Red (IR) cameras, a high resolution panchromatic camera operating in the visible spectral band and a color camera. In particular, while the other optical sensors have been used in experiments relevant to obstacle identification and flight in low visibility conditions, the panchromatic camera has been selected to test data fusion for autonomous non-cooperative collision avoidance, in a reduced field of regard (depending on camera field of view). However, this suffices for technology demonstration in quasi frontal near collision encounters, which represent the most challenging conditions. The sensing system is completed by a CPU devoted to image processing, and a CPU devoted to real time tracking. The real time tracking unit is connected by a CAN bus to the onboard Flight Control Computer that performs autonomous navigation, based on different sensors including a commercial-off-the-shelf Attitude and Heading Reference System (AHRS) with magnetometers and latest generation MEMS-based accelerometers and gyroscopes, and flight control including autonomous collision avoidance. The hardware architecture of the whole flight system is depicted in Fig. 1. The reader is referred to [14,20,21] for further details.

As main features, the adopted data fusion architecture is based on the concepts of hierarchy among sensors, central-level fusion [27], and cross-sensor cueing [14]. In fact, given the dependency of

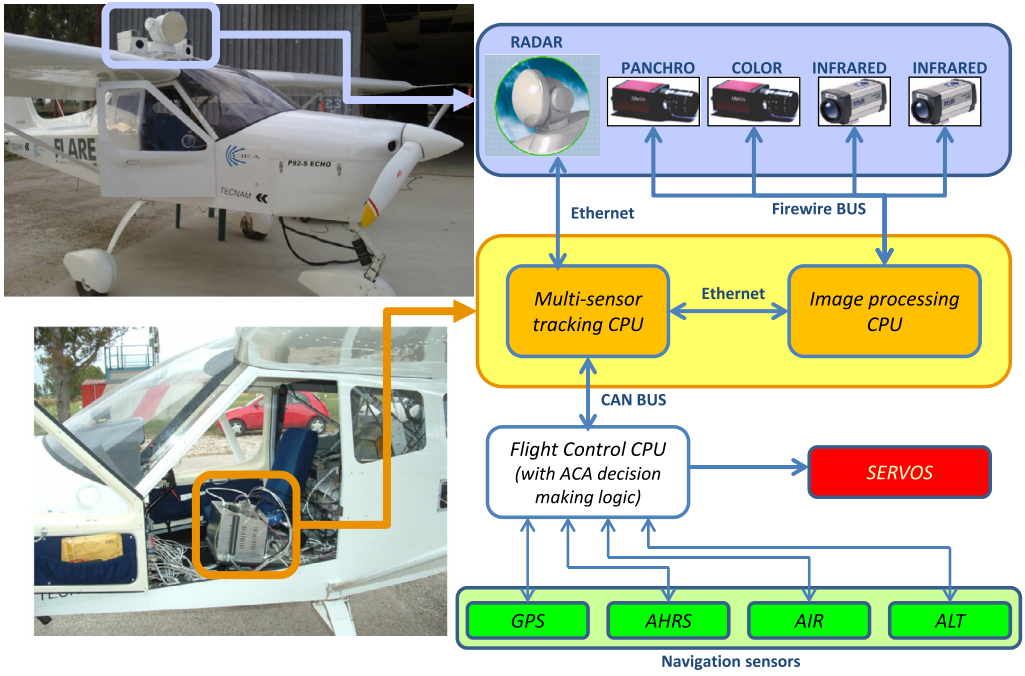

Fig. 1. Sense and avoid system hardware architecture, and FLARE aircraft (ACA: Autonomous Collision Avoidance; AIR: AIR data sensors; ALT: laser ALTimeter).

EO detection performance on environmental conditions, the radar is used as the main sensor that performs initial detection and tracking and determines track status, while the EO sensors in general are used as auxiliary information sources to increase accuracy and measurement rate. On the other hand, standalone radar tracking estimates can be effective in reducing the computation time and the false alarm rate of EO image processing. Thus, another important feature of the developed system is cross-sensor cueing, i.e., the exchange of information at sensor level, with the EO system that is cued by the tracking module. Cross-sensor cueing allows exploiting all the available information at sensor level, establishing a feedback mechanism between data fusion estimates and raw detections which can be the real added value of multi-sensor systems, besides the accuracy increase brought by the combination of measurements with different uncertainties.

The selected sensor fusion architecture is central-level: apart from pre-processing operations, raw sensor data are combined on the basis of their estimated uncertainty in a unique tracking algorithm based on an Extended Kalman Filter (EKF) [28], and no tracks are generated at sensor level. EKF constitutes a commonly used solution for filtering and prediction [15], but other fusion algorithms more suited for dealing with non-linear and/or non-gaussian systems such as the Unscented Kalman Filter (UKF), the Particle Filter (PF), and the recently developed Cubature Kalman Filter (CKF) [29] could also be used and are under analysis [30]. The potential of these approaches in terms of tracking performance has to be traded-off against computational burden which can hinder real time implementation (especially for PF), though the continuous performance improvements of on-board computing systems tend to reduce these issues. On the other hand, a key aspect to consider is the reliability in different scenarios (possibly with a few valid measurements to exploit) without an excessive dependence on ad hoc tuning. Of course, multi-sensor systems are the best candidate for implementing these techniques because of their potential in terms of detection accuracy and measurement rate. While a comparative analysis of different filtering schemes is beyond the scope of this paper, future works will address these topics.

The logical architecture of the multi-sensor-based obstacle detection and tracking system is outlined in Fig. 2. The following sub-sections focus on challenges and solutions for effective real time data fusion, and the flight-based procedure adopted for high accuracy sensors' alignment estimation. The implemented EO obstacle detection algorithm is described in detail in [21].

3.1. Real time multi-sensor tracking

The multi-sensor tracking algorithm enables effective fusion of the information provided by the different sensors and allows estimating obstacle kinematics. It runs at 10 Hz to properly follow ownship dynamics and is based on an EKF with linear dynamic model and non-linear measurement equation. The state vector is comprised of nine components which are obstacle coordinates in NED (North-East-Down reference frame with origin in the aircraft center of mass) with their first derivatives and the NED components of target acceleration. A classical Singer model is used for the three acceleration components [31,32] which assumes that every component of target acceleration evolves in terms of a correlated noise process with given time constant and instantaneous variance, i.e., in discrete terms it is modeled as

$$a(k+1) = \rho_m a(k) + \sqrt{1-\rho_m^2}\sigma_m r(k) \tag{1}$$

where σ_m^2 is the acceleration instantaneous variance, μ is the inverse of target acceleration time constant, $\rho_m = \exp(-\mu T)$ with T being the sampling interval, and $r(k)$ is a zero-mean unit-standard deviation Gaussian random variable [20].

The model is flexible since it is possible to control the filter bandwidth by tuning the process noise matrix. Given the key requirement of tracking reliability, the choice has been to keep a relatively large filter bandwidth to minimize the risk of biases generation and consequent track loss. Indeed, this increases in some way the risk of including EO false alarms within the filtering process, with possible bad association and consequent track degradation. Moreover, within the integrated radar/EO system tracking reliability can be more severely affected by EO false alarms than by missed detections. Thus, a rather conservative tuning of the EO obstacle detection algorithms is considered.

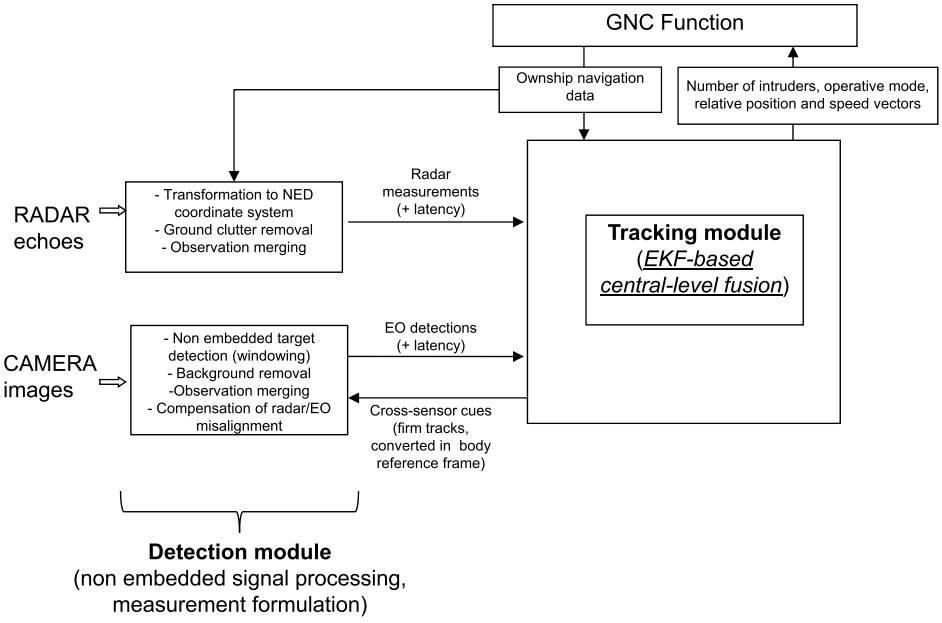

Fig. 2. Logical architecture of multi-sensor-based obstacle detection and tracking system.

As regards measurement equation, the angle-related entries of measurement covariance matrices depend not only on radar and EO performance but also on AHRS inaccuracies in estimation of aircraft attitude angles. Since flight data offer a precise characterization of angular errors in NED (reference given by GPS data only) measurement covariance can be estimated using sensor data gathered in data collection flights. The impact of attitude measurement errors can be more detrimental for the EO sensors than for the radar, since the finer angular resolution can be more significantly degraded in the process of measurement formulation in NED. It is also important to underline that it is mainly the attitude measurement noise that impacts measurement covariance, while nearly constant errors are less important for collision avoidance aspects. Besides attitude measurement uncertainty, measurement formulation in NED for EO systems is influenced by frame rate, image timing accuracy, and actual aircraft attitude dynamics.

Track/measurement association is carried out using ellipsoidal gating and a centralized statistic [28]. In order to improve EO sensors performance and reliability and to reduce the computational load, EO detection process is carried out in a window centered in the foreseen intruder position. EO-based detection algorithm takes advantage from cross sensor cueing in different ways [21]:

- Center of search window located by coarse estimation of intruder line of sight;
- Range based selection of search window dimensions;
- Adoption of range dependent criteria for defining image processing thresholds and applying consistency checks on candidate measurements.

If the image processing system successfully detects an intruder, the EO measurement is used only if satisfies the gating process. It has to be considered that during radar/EO tracking track covariance is reduced with respect to radar-only tracking, so that false alarms are likely to fall outside the gate and in such case are discarded and do not affect track accuracy. Indeed, the risk of EO false alarm filtering is higher in the first phase of firm tracking, when track covariance is still large because of the radar rough angular accuracy.

When considering real time implementation of developed data fusion algorithm, important issues are related to proper management of sensors' latency and accurate space registration of their measurements. While the first point is discussed here, the second one is analyzed in Subsection 3.2. As documented by the manufacturer, radar latency can be at most of the order of 1 s for the considered settings, and measurement delay is provided by the sensor for each detection. Since the tracker works at 10 Hz, in the developed system a measurement is assigned a time stamp which is the nearest time on the tracker 0.1 s scale. Then, to perform gating, association and track updating, the solution is to keep in memory a sliding window where navigation and track data are stored. The considered time window dimensions correspond to the largest possible radar data latency. This also implies that the maximum acceptable latency for the EO system is on the order of 1 s. EO latency is computed by the tracking software because both track data sent to the image processing unit and the eventual positive replies are time-tagged: measurements with larger latency than 1 s are automatically discarded. However, image processing latencies, estimated first in laboratory hardware-in-the-loop [33] and then in flight tests, were of the order of 0.1 s at most.

For EO and radar measurements, filtering process consists in evaluating filtered state and covariance at measurement time and then in modifying current state and covariance on the basis of this information, based on the linearity of the tracking filter [20]. In general, latency of EO detection depends on the computational load of image processing, while radar delay depends on the intruder position in the radar scan volume. As a consequence, when both sensors provide reliable detection, it is likely to have out-of-sequence measurements (OOSM) which is a well known problem in real time multi-sensor tracking [28,34]. Due to the operating scenario, it is unlikely to have more than one or very few firm tracks, so it is possible to handle OOSM without any approximation, by using stored track data and re-filtering measurements if necessary, since the computational burden is compatible with real time implementation. In this way measurements are used as soon as possible and at the same time no loss of accuracy is produced. From the programming point of view, this means that a sliding window is kept in memory also to store sensor measurements for possible re-filtering.

A qualitative example of OOSM processing is shown in Fig. 3. At a given time, current state and covariance estimates have been generated (a). When a delayed EO measurement arrives, state and

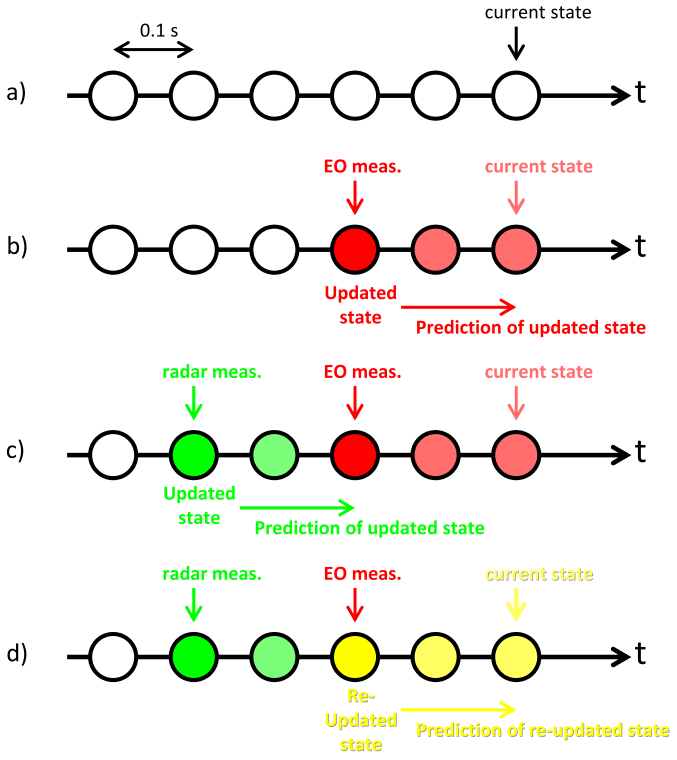

Fig. 3. Qualitative example of out-of-sequence measurements processing for state estimation (the same logic applies to covariance calculations). Colors are used to clarify state estimates dependency on sensor measurements. (For interpretation of colors in this figure, the reader is referred to the web version of this article.)

covariance updates are calculated at measurement time and then propagated to the current time (b). If an out-of-sequence radar measurement arrives, first state and covariance updates are calculated at radar measurement time and propagated to the EO measurement time (c), then the EO measurement is used again within the filtering algorithm, and state and covariance updates are again propagated to the current time (d).

3.2. Flight-based relative sensors alignment

In general, a key point for effective sensor fusion is accurate spatial registration among the sensors [28]. In the considered system, all the EO sensors can be aligned with high accuracy with respect to the AHRS by means of a ground procedure based on carrier phase differential GPS measurements, own EO image processing, and least squares optimization [35] which permits to attain an rms alignment accuracy on the order of 10^{-1} degrees. The same ground procedures cannot be applied for the radar: in this case fine alignment with respect to the AHRS can be based on flight data analysis. In particular, chasing phases can be effectively used thanks to the large number of intruder detections, smooth relative dynamics, and consequent small impact of latencies. However, implementing these two separate procedures, based on ground and flight data, can have some limitations for the estimation of relative alignment if a commercial MEMS-based AHRS, such as the one embarked on FLARE, is used. In fact, attitude measurement error in dynamic conditions differs from the one achievable in static conditions. Besides attitude error noise, error biases (above all, heading error) can differ because of residual uncompensated magnetometer biases and onboard magnetic fields (due for example to engine operation), which produce measurement errors depending on aircraft orientation in the Earth magnetic field.

Thus, a flight-based calibration procedure has been developed whose aim is to estimate with high accuracy the relative alignment between radar and EO cameras. In fact, a common alignment error of both radar and EO sensors with respect to AHRS does not impact significantly collision avoidance capabilities, since it is equivalent to an error bias in attitude angles measurements and as such it does not affect computation of angular derivatives of intruder motion. On the other hand, relative misalignment has detrimental effects on collision detection capabilities since it generates measurements with different biases, whose effects depend on the story of intruder detections and are thus unpredictable *a priori*. From a practical point of view, angular derivatives of intruder motion can be affected which are the most important variables for accurately estimating collision risk. The flight-based alignment procedure can be carried out combining ownship and intruder navigation data, radar measurements, and optical images, as shown in the flow chart depicted in Fig. 4.

A flight segment has to be considered whose duration is of the order of some tens of seconds and which is characterized by chasing flight and no significant variations of heading angle. Within this flight segment, it is assumed that biases in attitude angles errors are nearly constant, especially regarding the heading angle. This assumption can then be verified by the analysis of radar/optical azimuth and elevation errors. The intruder has to be at a minimum distance of several hundreds of meters, so that GPS linear positioning uncertainty is mitigated in angular terms. Within this framework, uncertainty in reference GPS measurements can be lowered by exploiting satellite-based or ground-based augmentation systems for the ownship and/or the intruder [36]. From a geometric point of view, it is preferable that scans/frames are processed with the intruder lying in different areas of the sensor FOVs, in order to guarantee the same level of accuracy on all Euler angles.

Radar and EO measurements refer to different times and direct measurement interpolation can introduce significant additional errors considering that measurements are generated in sensors' reference frame and that measurement rate is low, especially for radar. However, the assumption of stationarity of attitude error biases allows indirect estimation of relative sensor alignment. In fact, radar and EO alignment matrices with respect to the AHRS can be calculated separately.

Considering for example the radar, first of all, for each measurement linear interpolation of GPS data (available at a frequency of 1 Hz) allows the intruder relative position vector in NED at the considered measurement instant to be found. Then, interpolation of attitude data (available at 10 Hz) and subsequent transformation by the aircraft attitude matrix gives the relative position vector in BRF. Let us call this vector $\underline{r}_{iBRF}$, where the i index refers to the generic i-th measurement. Dividing by its modulus, it is possible to evaluate the cosine directors of the line-of-sight to the target relevant to the radar and the i-th measurement. Let us call $\hat{\underline{r}}_{iBRF}$ the computed unit vector. Target position vector as given in radar output can be used first of all to select echoes that can be associated with very good confidence to the intruder, i.e. echoes that have differences in range, azimuth and elevation below assigned thresholds. If this is the case, it is possible to define $\hat{\underline{r}}_{iRAD}$ as the unit vector representing the direction to the target in the radar based reference frame relevant to the i-th scan (at most a single measurement can be associated to the intruder in each scan). It is then possible to define a loss function:

$$J(M_{RAD}) = \sum_{i=1}^{n} w_i |\hat{\underline{r}}_{iRAD} - M_{RAD}\hat{\underline{r}}_{iBRF}|^2 \tag{2}$$

where n is the number of collected measurements/positions, w_i is the weight of the i-th measurement and M_{RAD} is the alignment matrix of the radar with respect to the aircraft. The loss function is thus the weighted sum squared of the differences between the

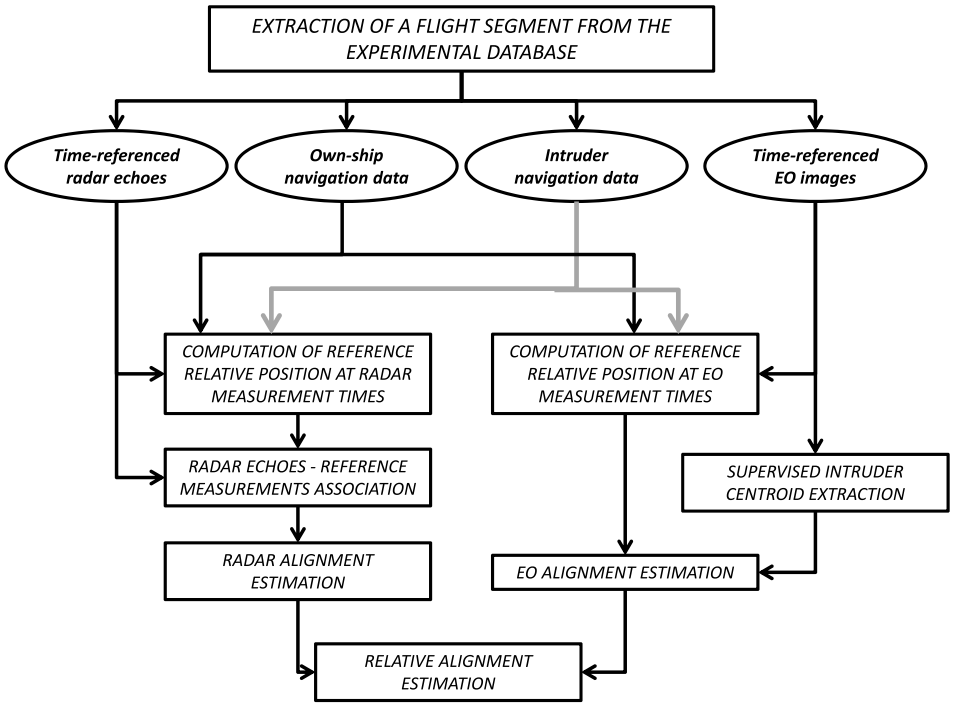

Fig. 4. Flow chart of the flight-based relative alignment procedure, assuming supervised intruder extraction from EO images.

measured and transformed vectors. An optimal choice of M_{RAD} is that which minimizes J. It can be computed by means of the algorithm named q-method which calculates attitude in terms of the corresponding optimal least-square quaternion [37]. The weights are linearly related to intruder range to take into account the variable impact of GPS linear uncertainties on estimated angles.

A similar procedure can be used for the EO cameras, and in particular for the panchromatic one, in order to get a rotation matrix M_{CAM}. In this case, supervised image analysis (or the obstacle detection algorithm fed by GPS/AHRS cues) allows target center pixel to be identified in each image, which is then translated into angular information by exploiting the camera intrinsic parameters.

Once the two matrices are calculated, under the above mentioned assumption of stationary error biases relative alignment matrix can be obtained by a matrix product, i.e.

$$M_{RAD\to CAM} = M_{RAD}^{T} M_{CAM} \tag{3}$$

Though the single unit vectors are affected by aircraft dynamics and attitude error noises, the large number of samples available from flight data can reduce the estimation uncertainty, while generating a robust estimation of relative sensors alignment.

4. Flight results

The sense and avoid flight test campaign carried out within TECVOL project comprised several different tests. This paper deals with results from the obstacle tracking experiments (autonomous anti-collision logic not engaged) and aims at comparing standalone radar tracking with radar/EO tracking output. In particular, the comparison is carried out exploiting both flight data and off-line simulations based on a software which faithfully replicates the real time tracking module. All flight tests were carried out with a configuration of test facilities comprising FLARE aircraft piloted by human pilot or by the autonomous flight control system, a piloted intruder VLA equipped with GPS, a Ground Control Station (GCS) for real-time flight coordination and test monitoring, a full-duplex data-link between FLARE and GCS, and a downlink between intruder and GCS. Two types of maneuvers were basically executed during flight experiments, such as chasing tests with FLARE pursuing the intruder (useful for flight-based relative sensor alignment), and near collision encounters.

Flight results are presented as follows. First, flight-based relative sensor alignment results are described which allow the multi-sensor tracking algorithm to be properly tuned and thus to reach the best performance. Then, main aspects of detection performance by radar and EO camera are recalled, and tracking results are analyzed. Finally, estimation of situational awareness is focused to better point out the performance increase due to data fusion, and the key points for fusion effectiveness.

4.1. Flight-based alignment

An example of flight-based alignment is here reported considering a chasing flight segment of about 80 s, with FLARE keeping an almost constant heading angle and intruder range increasing from 700 m to about 2 km. While attitude measurement error biases are with good approximation constant, the duration of the considered flight segment and the smooth relative dynamics allow having a significant number of radar/optical detections to be exploited by the alignment algorithm.

For the sake of clarity, Fig. 5 reports intruder range as estimated from GPS data, and radar echoes in the considered flight segment. A portion of a panchromatic image comprising the intruder (at a range of about 830 m) is also reported.

Extracting (by means of a supervised procedure) intruder pixels from images, individuating radar echoes due to the intruder, and applying the previously described alignment procedure leads to the "absolute" (i.e., with respect to the AHRS) and relative alignment angles reported in Table 1. The Euler angles are all relevant to a heading-pitch-roll sequence. It is worth underlining that absolute alignment angles are not used by the tracking software (absolute misalignment has no impact on collision detection capabilities and AHRS biases are variable in different flight segments).

As a first estimate of procedure uncertainty, Figs. 6 and 7 report the angles between intruder unit vectors as measured from scans/images and the same vectors as generated from GPS/AHRS

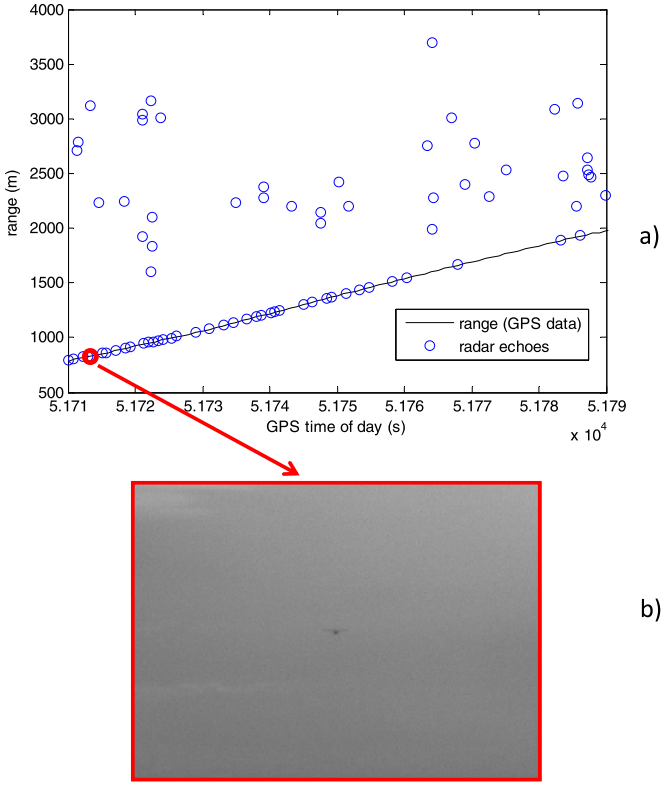

Fig. 5. (a) Chasing flight segment used for flight-based relative radar/EO alignment: range as estimated by GPS and by radar, (b) zoom of an image window enclosing the intruder aircraft at a range of about 830 m.

Table 1
Absolute and relative alignment angles estimated from flight data.

Estimated angle (°)	Radar w.r.t. BRF	Panchromatic camera w.r.t. BRF	Radar w.r.t. panchromatic camera
Heading	0.32	1.19	−0.86
Pitch	0.49	0.64	−0.16
Roll	−1.12	−0.51	−0.61

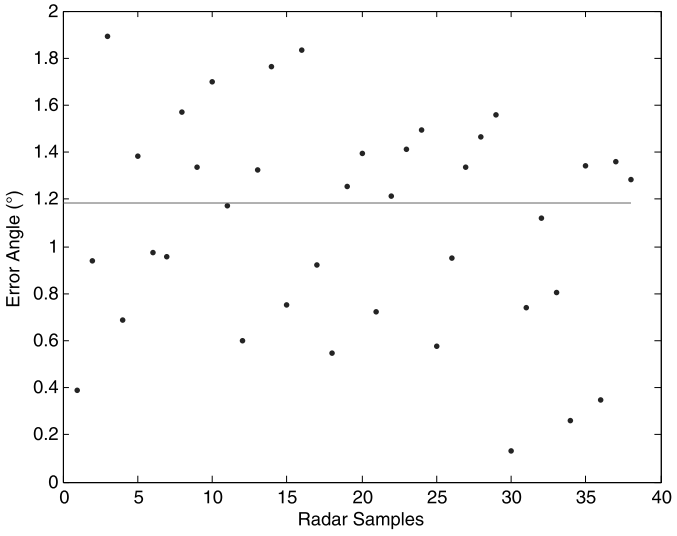

Fig. 6. Error angle between the intruder unit vector as measured from radar scans and the same vector as generated from GPS/AHRS data and estimated radar alignment matrix, for all the considered samples.

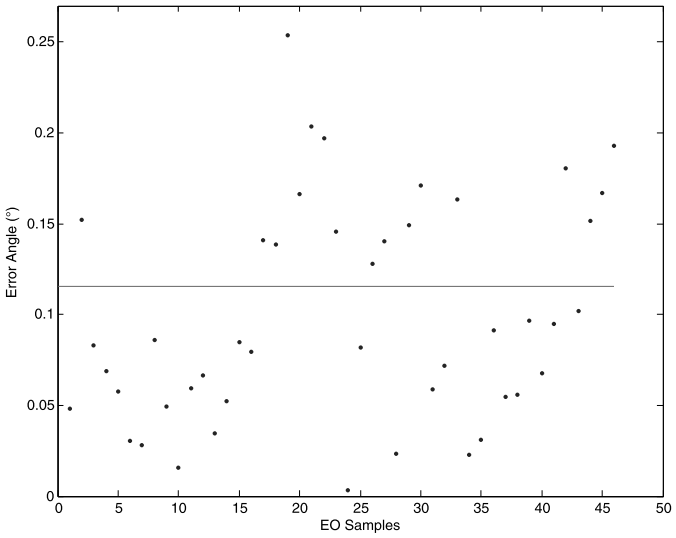

Fig. 7. Error angle between the intruder unit vector as measured from EO camera images and the same vector as generated from GPS/AHRS data and estimated camera alignment matrix, for all the considered samples.

data and estimated (absolute) alignment matrices. It can be seen that no significant systematic error trends can be identified in the diagrams. In both diagrams, the root mean square (rms) value of the angle over all the samples is also depicted. It can be seen that the value obtained from the radar is of the order of the beamwidth of its antenna main lobe, while in the case of the panchromatic camera the obtained rms angle is of the order of 0.1°, not significantly more than camera Instantaneous Field Of View (IFOV, about 0.040°), which confirms the stability of attitude error biases during the processed flight segment. As it will be evident from multi-sensor fusion results too, this can also be assumed as the order of magnitude of the residual uncertainty in relative sensor alignment, enabling accurate registration of radar echoes and camera-based estimates.

4.2. Detection and tracking performance

The radar was confirmed to be a reliable source of information with a detection range of about 3 km in different conditions (unambiguous range was set to be 4 km in the considered tests) and a coarse angular accuracy of the order of its antenna main lobe, i.e. 1.7°. A great amount of ground echoes were detected due to the limited flight altitude (a few hundreds of meters), while the valid measurement rate was of less than 1 Hz on average [20].

Regarding obstacle detection by the EO camera in the integrated multi-sensor system, cross-sensor cueing plays a key role for reducing performance sensitivity on environmental conditions and improving EO detection performance while keeping a small computational burden. An example of the highly variable operating conditions for the EO system (in terms of background homogeneity and intruder appearance) is shown in Fig. 8 which depicts two images enclosing the intruder at a distance of about 1 km in different illumination conditions (sun in front at the limits of camera FOV, and sun in the back, in mean visibility conditions). The intruder aircraft is brighter than the background in one case, and darker in the other. In the sun-in-front case, main issues for correct intruder detection are relevant to sun glare effects and contrast reduction, while in the sun-in-the-back case they are related to the reduction of background homogeneity and to the presence of many small white clouds which can be erroneously taken as the intruder aircraft. In fact, in spite of these challenging operating conditions, in mean visibility conditions image windowing and exploitation of range estimate enable reliable detection at a range larger than

Fig. 8. Panchromatic images taken in different illumination conditions. The arrows point to the intruder aircraft, at a range of about 1 km in both cases.

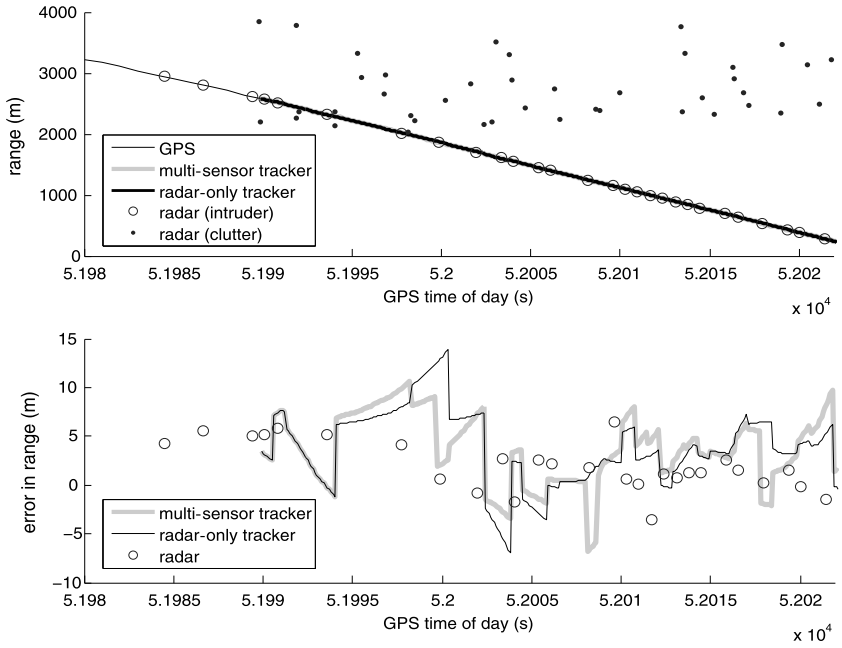

Fig. 9. Range (GPS, multi-sensor tracker, radar-only tracker, and radar) and relative estimation error (multi-sensor tracker, radar-only tracker, and radar) as a function of GPS time in considered scenario.

2 km for an ultralight aircraft [21]. In addition, false alarm rate is kept at a very small value by conservative tuning of the algorithm. This is paid with a very slight increase of missed detection rate at large range, and the impact of the residual false positives is mitigated by the multi-sensor tracking architecture which foresees gating.

Regarding obstacle tracking performance, in general it depends on the considered relative dynamics scenario. From the application point of view, quasi-frontal near collision geometries are of course the most interesting ones. These geometries are characterized by fast relative dynamics and short time duration, and a few radar detections can be typically exploited for tracking, while EO data offer the potential of a significant increase in measurement rate. Indeed, in the considered flight tests EO data were acquired and processed at 3.3 Hz due to limitations on the mass memory of the image processing unit, thus radar/EO data fusion can be performed at this maximum frequency. In any case this constitutes a significant improvement compared with radar-only tracking, where valid intruder detections are received at a frequency of less than 1 Hz, on average.

In order to estimate tracking performance, GPS measurements (differential GPS for FLARE aircraft, standalone GPS for the intruder aircraft) are used as reference, and GPS time is used as reference time for synchronization. Azimuth, Elevation, Azimuth rate, and Elevation Rate estimates are all expressed in a stabilized NED reference frame with origin in FLARE center of mass. In this way, AHRS measurements of attitude angles and the relevant uncertainties are not used to compute reference values.

In what follows, a single near collision encounter is analyzed in detail. The considered scenario is characterized by a closing speed which increases in the very first part of the encounter (when the two aircraft are smoothly maneuvering) until reaching an almost constant value of about 75 m/s, and a range of about 2.95 km at first detection, corresponding to a time-to-CPA of about 45 s. Firm tracking phase is entered at a range of about 2.6 km. The illumination conditions are characterized by the presence of the sun in front of FLARE aircraft and by average visibility conditions. Moreover, the intruder flies near the horizon line in the initial part of the considered encounter.

Outputs of tracking algorithm in single sensor and multi-sensor configuration are presented in Figs. 9–14 which also report raw sensor outputs where applicable, GPS-based estimates, and sensors/tracking errors. In these diagrams, radar echoes that can be associated with very good confidence to the intruder (empty circles) are separated from clutter returns (filled points) by verifying that differences in range, azimuth and elevation with respect to

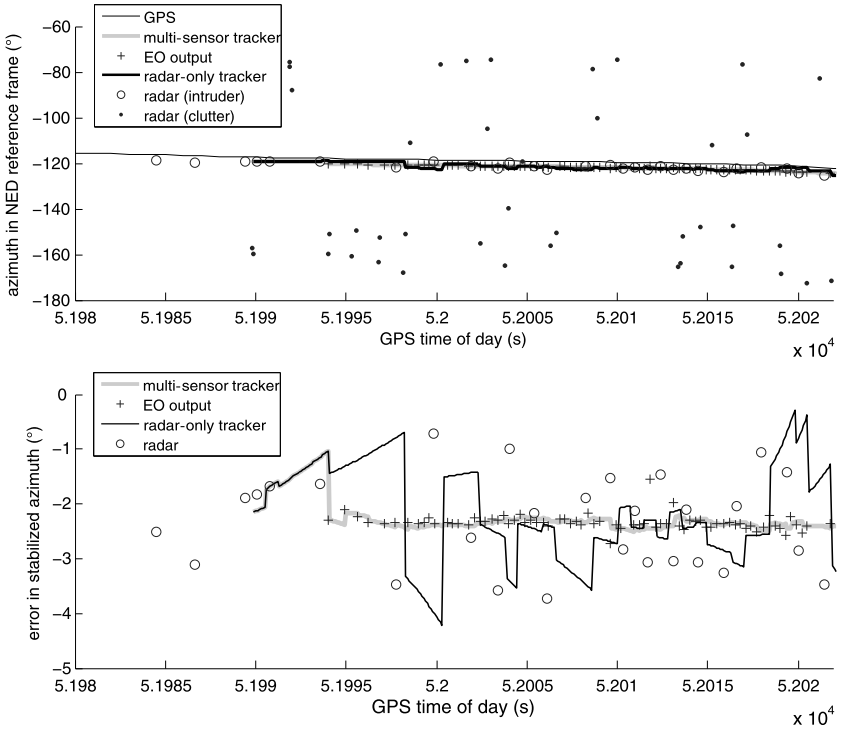

Fig. 10. Stabilized azimuth (GPS, multi-sensor tracker, EO, radar-only tracker, and radar) and relative estimation error (multi-sensor tracker, EO, radar-only tracker, and radar) as a function of GPS time in considered scenario.

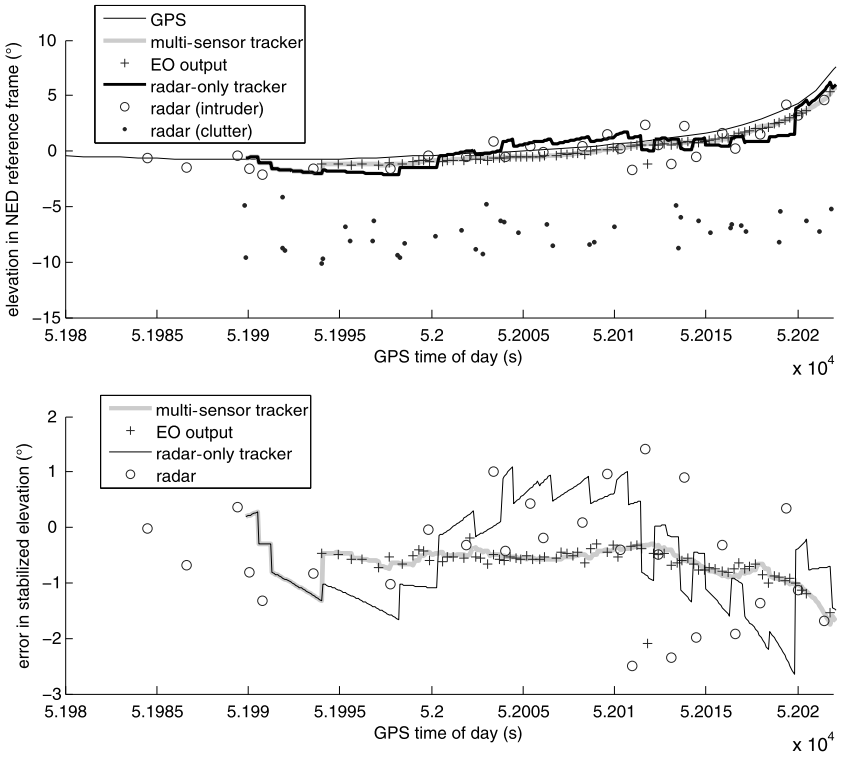

Fig. 11. Stabilized elevation (GPS, multi-sensor tracker, EO, radar-only tracker, and radar) and relative estimation error (multi-sensor tracker, EO, radar-only tracker, and radar) as a function of GPS time in considered scenario.

GPS-based estimates fall below assigned thresholds. This is also required to carry out a quantitative analysis of radar accuracy.

As expected, the range estimates (Fig. 9) are not very much affected by EO measurements, with only some small effects due to the range-angles coupling introduced by the Cartesian dynamic model used in the tracking filter. The multi-sensor and the radar-only tracker outputs are very similar to each other, with an accuracy of the order of a few meters which derives from the fine radar range accuracy. Due to the limited flight altitude, a significant number of ground echoes is detected (at negative elevation angles, as shown in Fig. 11), which are correctly removed in real time by the tracking algorithm on the basis of their estimated

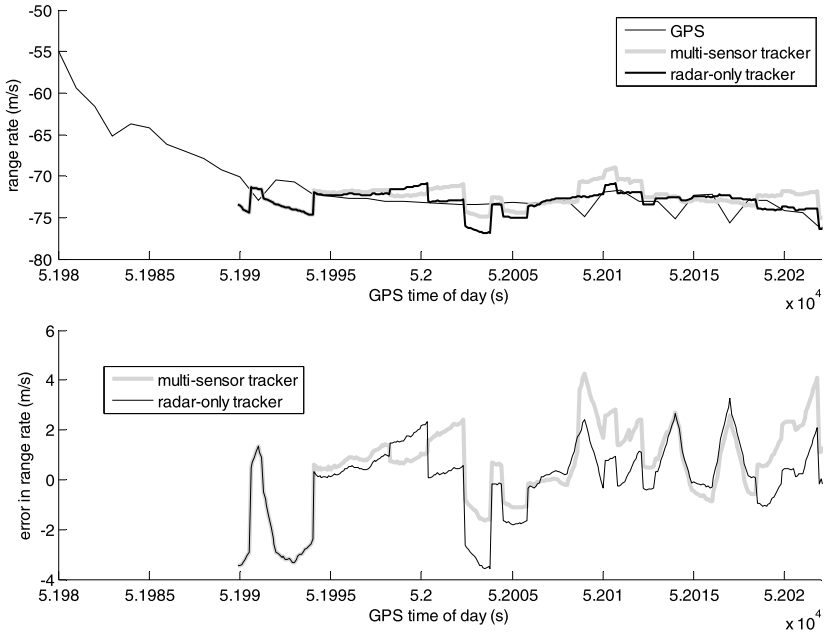

Fig. 12. Range rate (GPS, multi-sensor tracker, and radar-only tracker) and relative estimation error (multi-sensor tracker and radar-only tracker) as a function of GPS time in considered scenario.

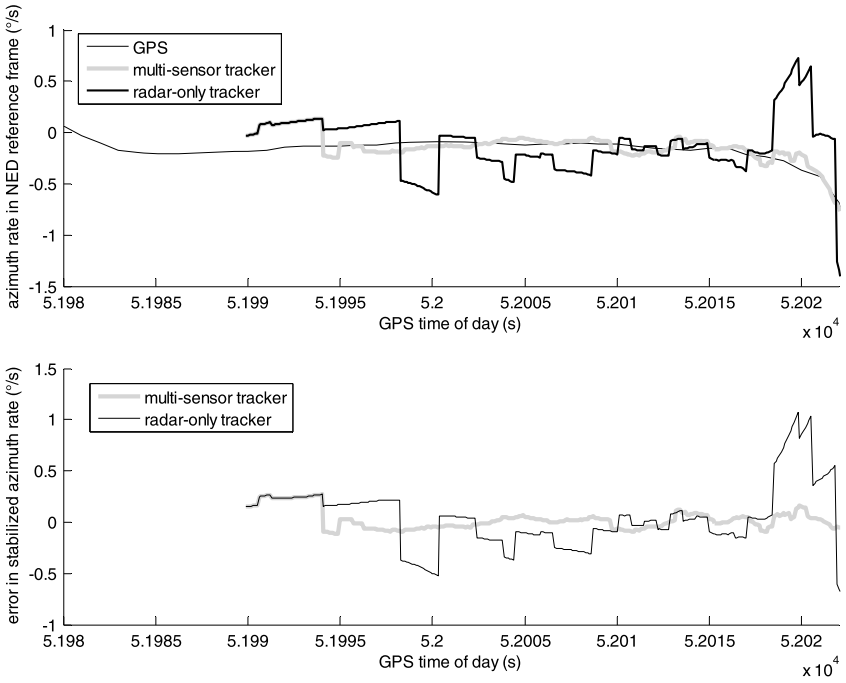

Fig. 13. Stabilized azimuth rate (GPS, multi-sensor tracker, and radar-only tracker) and relative estimation error (multi-sensor tracker and radar-only tracker) as a function of GPS time in considered scenario.

range and altitude [20], and have no effects on tracking performance.

The diagrams relevant to angular estimates (Figs. 10 and 11) show significant differences between the multi-sensor and the single sensor tracker, and offer several discussion points.

First of all, a significant number of valid measurements is provided by the EO system and used by the tracking algorithm in the multi-sensor case, in spite of the limited frame rate and the challenging illumination conditions, with a single larger error estimate (GPS time of day of about 52 012 s) which represents a false positive. Both radar and EO measurement errors show significant biases in azimuth (about $-2.2°$) and in elevation (about $-0.6°$), which are with good approximation constant during the considered encounter. In the elevation case, this is due to the residual misalignment between AHRS and obstacle detection sensors. In the azimuth case, the phenomenon is due to the combination of residual misalignment and the bias in estimation of aircraft heading angle, which depends on vehicle orientation in Earth magnetic field and in general is due to several issues, such as:

- magnetometers sensitivity and calibration residual inaccuracies;
- uncertainties in modeling Earth magnetic field;
- residual uncompensated magnetic fields.

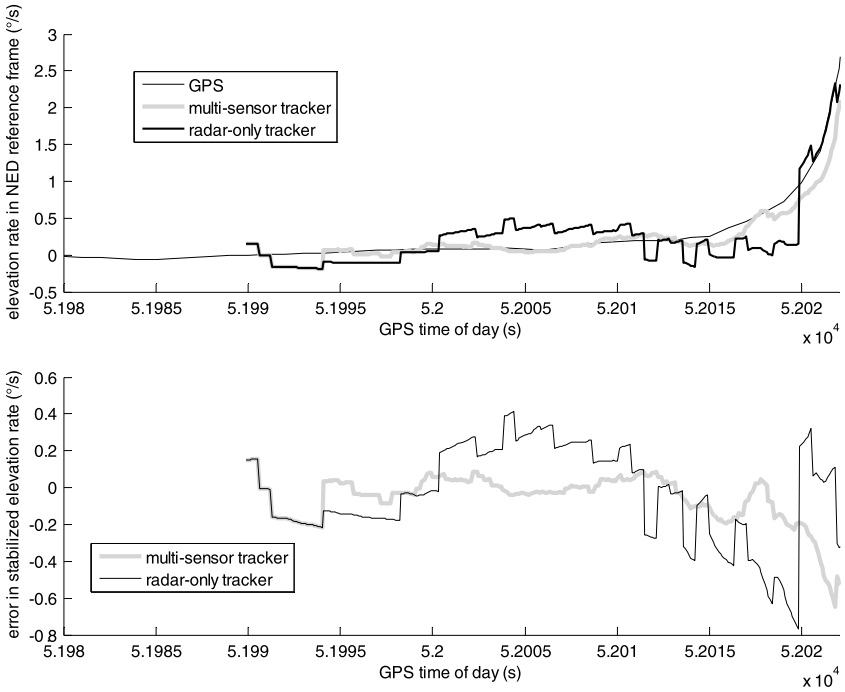

Fig. 14. Stabilized elevation rate (GPS, multi-sensor tracker, and radar-only tracker) and relative estimation error (multi-sensor tracker and radar-only tracker) as a function of GPS time in considered scenario.

As stated above, no AHRS-radar and AHRS-camera alignment corrections are applied within the multi-sensor tracking algorithm, which is due to the fact that these biases are constant (elevation) or variable (thus not removable in flight) but slowly time varying in each flight segment (azimuth), with little or no consequences on intruder velocity predictions and collision avoidance safety.

Instead, it is important to underline that radar and EO biases are the same both in azimuth and in elevation, within an approximation of about 0.1°. This confirms that quality of relative sensors alignment is very high with a residual uncertainty of that order of magnitude. Furthermore, image timing accuracy, and more in general time registration errors, are confirmed not to affect system performance at a significant level, though FLARE, being a small aircraft, exhibits a very "noisy" attitude dynamics also due to lateral directional flight dynamics modes excited by radar inertia and mechanical scanning operation.

Comparison of raw sensor measurements allows pointing out the different performance level of radar and camera both in terms of error standard deviation (of the order of 1° for the radar, 0.15° for the camera) and valid measurement rate (on average after the first detections, about 0.7 Hz for the radar, about 2.6 Hz for the camera). Regarding angular error noise in NED, it is interesting to note that, consistently with the results of flight based alignment, camera accuracy is not degraded at a significant level compared with its IFOV, though a commercial MEMS-based AHRS system is used.

Considering now the outputs of the tracking algorithm, both in azimuth and in elevation there is a great difference between the radar-only and the multi-sensor tracker, and the impact of radar/EO fusion on performance is dramatic: in the multi-sensor case, while accuracy is significantly increased, almost achieving at a frequency of 10 Hz the order of magnitude of EO angular errors (error standard deviation is of about 0.3°), tracking outputs also gain a great advantage from EO measurement rate generating smoother estimates. It can also be appreciated that the single false positive provided by the image processing system does not negatively impact performance, since it falls outside track gate and thus is discarded in track filtering phase. On the other hand, radar-based tracking outputs are reliable but in terms of accuracy they suffer from both rough angular error and low valid measurement rate. In this case, error noise is of about 0.9° both in azimuth and in elevation, about three times the accuracy of multi-sensor-based estimates. As expected, both tracking algorithms generate biased outputs which directly derive from raw measurements biases. As a final remark to the angle diagrams, both for raw measurements and for tracking outputs a somewhat larger angular error can be individuated in the very last instants before encounter, especially in the elevation case because of the encounter geometry with almost zero lateral separation. Nevertheless, this corresponds to a very small positioning error and is due to the fact GPS is not a very accurate reference at very small ranges due to the impact of residual time synchronization and linear positioning uncertainties.

Analysis of the derivatives gives further insight into tracking behavior. Depending on range accuracy, tracking error in range rate (Fig. 12) is of the order of 1 m/s during the whole encounter for both the radar-only and the multi-sensor tracker, with no significant impact of radar/EO fusion. Also considering that no significant error biases are exhibited, this performance level largely suffices for the needs of collision detection and avoidance.

In view of collision detection performance, angular rates (Figs. 13 and 14) are the key variables which gain advantage from data fusion. In both the radar-only and the multi-sensor case, as a consequence of constant angle error biases, azimuth and elevation rates are with good approximation unbiased, a general result that was experienced in the whole flight test campaign. However, in the multi-sensor case, the increase of accuracy and measurement rate brought by EO detections optimally integrates radar-based information and allows the tracking algorithm to significantly improve angular rate performance, so that the azimuth rate and the elevation rate errors fall below 0.1°/s for almost the whole encounter duration, with the exception of the very last instants as explained above. Compared with average radar-only tracking accuracy (root mean square error of about 0.3°/s both in azimuth and in elevation), as in the angular case this represents a reduction by two-thirds of the error, which is achieved in spite of the limitations of the experimental setup such as limited frame rate. In fact,

Table 2
Statistics of sensors and trackers errors in the considered frontal encounter.

	Range (m)	Azimuth (NED) (°)	Elevation (NED) (°)	Range rate (m/s)	Azimuth rate (NED) (°/s)	Elevation rate (NED) (°/s)
Radar mean (<1 Hz)	1.9	−2.3	−0.50	N/A	N/A	N/A
Electro-optical mean (<3 Hz)	N/A	−2.3	−0.60	N/A	N/A	N/A
Radar-only tracker mean (10 Hz)	3.8	−2.3	−0.52	−0.064	0.037	−0.035
Multi-sensor tracker mean (10 Hz)	3.6	−2.2	−0.60	0.41	0.029	−0.035
Radar std (<1 Hz)	2.5	0.86	1.0	N/A	N/A	N/A
Electro-optical std (<3 Hz)	N/A	0.10	0.18	N/A	N/A	N/A
Radar-only tracker std (10 Hz)	3.9	0.88	0.92	1.6	0.29	0.26
Multi-sensor tracker std (10 Hz)	3.6	0.31	0.26	1.6	0.099	0.092

an even more significant tracking performance improvement could be expected for the given camera angular resolution by exploiting a larger frame rate.

To summarize the results of the analysis, statistics of sensors and tracking errors (mean and standard deviation) are reported in Table 2. In order to limit the effect of linear GPS and data synchronization errors when transformed into angular uncertainties, these statistics have been evaluated considering only the flight segment when the range between the two aircraft is larger than 350 m. Statistics relevant to the multi-sensor tracking scenario also comprise the very first part of the encounter, when tracking output is based only on radar measurements. However, both error mean and standard deviation for the multi-sensor tracker are close to EO statistics, also as a consequence of the larger weight that EKF gives to optical measurements. As also noted in previous analyses [20], the tracker exhibits in range slightly larger uncertainties than the radar because of the impact of the slow measurement rate given the assigned flight geometry. These statistics confirm that data fusion combines in an optimal fashion the different sources, keeping practically the same range and range-rate accuracy of radar-based tracking while enabling a substantial improvement of angular and angular rate estimates.

4.3. Estimation of situational awareness

In order to focus the impact of this performance improvement for autonomous sense and avoid, it is worth recalling that non-cooperative obstacle detection and tracking are basically needed for collision detection, and for keeping situational awareness during (at least part of) the avoidance maneuver. Within this framework, the two main quantities of interest are the time to closest point of approach (t_{CPA}), also named time-to-go in literature, and the distance at closest point of approach (d_{CPA}), which is the basic variable for estimating collision risk [14] and can be evaluated in vectorial form on the basis of the knowledge of intruder relative position and velocity thanks to the equation

$$\vec{d}_{CPA} = \frac{\vec{r}\cdot\vec{V}}{\|\vec{V}\|^2}\vec{V} - \vec{r} = t_{CPA}\vec{V} - \vec{r} \tag{4}$$

where $\vec{r}$ is the relative position vector and $\vec{V}$ is the velocity vector of the UAS with respect to the intruder.

In the considered flight scenario, d_{CPA} computed on the basis of GPS measurements can be used as a reference for comparing the distance at CPA estimated by the radar-based and the multi-sensor tracker. This is shown in Fig. 15 that reports these estimates as a function of time until the actual closest point of approach, corresponding to a few tens of meters (and thus representing a real near mid air collision scenario).

Before discussing these results, it is useful to focus d_{CPA} sensitivity to angular rate errors. In near collision conditions, angular derivatives are the most important variables for collision risk estimation, since estimation errors correspond to erroneous rotations of the predicted relative velocity vector (indeed, a collision threat can be detected in absence of range information, given that angular rates are null and range rate is negative [11]). As an example, to estimate only the effect of an azimuth rate error $\varepsilon_{\dot{\varphi}}$ on d_{CPA} in near collision conditions, we can consider a simplified two-dimensional geometry with a frontal collision geometry and a given range rate [20], thus deriving

$$\varepsilon_{d_{CPA},\dot{\varphi}} = r\sin\left(\tan^{-1}\left(\frac{r\varepsilon_{\dot{\varphi}}}{|\dot{r}|}\right)\right) \approx t_{CPA} r\varepsilon_{\dot{\varphi}} \tag{5}$$

In the same way, an elevation rate error $\varepsilon_{\dot{\vartheta}}$ in near collision conditions gives

$$\varepsilon_{d_{CPA},\dot{\vartheta}} = r\sin\left(\tan^{-1}\left(\frac{r\varepsilon_{\dot{\vartheta}}}{|\dot{r}|}\right)\right) \approx t_{CPA} r\varepsilon_{\dot{\vartheta}} \tag{6}$$

At a first level of approximation, the d_{CPA} uncertainty due to the combination of the two angular rate errors can be evaluated assuming uncorrelated estimates as:

$$\varepsilon_{d_{CPA}} = \sqrt{\varepsilon^2_{d_{CPA},\dot{\varphi}} + \varepsilon^2_{d_{CPA},\dot{\vartheta}}} \approx \frac{r^2}{|\dot{r}|}\sqrt{\varepsilon^2_{\dot{\varphi}} + \varepsilon^2_{\dot{\vartheta}}} \approx t_{CPA} r\sqrt{\varepsilon^2_{\dot{\varphi}} + \varepsilon^2_{\dot{\vartheta}}} \tag{7}$$

Root mean square (rms) values of azimuth and elevation rate errors as estimated in radar-only and multi-sensor configuration, and GPS-based range and range rate measurements in the considered encounter, can be used within Equations (5)–(7) to derive uncertainty trends for d_{CPA}. Since mean angular rate errors are with good approximation null, rms values practically coincide with error standard deviations reported in Table 2. It is interesting to underline that, for constant range rate (typical near collision geometries) and given angular uncertainties (firm tracking phase for a given sensors/algorithms combination), equation (7) indicates a quadratic decrease of $\varepsilon_{d_{CPA}}$ with time, since range decreases linearly with time.

For the sake of clarity, radar and multi-sensor tracking uncertainties have been summed and subtracted to the reference d_{CPA} trend computed from GPS to obtain the diagrams depicted in Fig. 15, which also reports t_{CPA} as estimated by GPS and by the two tracking algorithms. Uncertainty envelopes are depicted only for positive values since d_{CPA} by definition cannot be a negative quantity.

While t_{CPA} is estimated accurately by both trackers (rms difference with respect to reference 0.34 s for multi-sensor and 0.41 s for radar-only tracker) as a consequence of fine radar range accuracy, the difference in d_{CPA} diagrams clarifies the remarkable increase in the level of situational awareness that is achieved in multiple sensor configuration. In fact, both trackers demonstrate a reliable behavior though the reference d_{CPA} is not constant, demonstrating as anticipated above that the two aircraft are smoothly maneuvering especially in the first part of the collision scenario. However, soon after the first EO detection (at a relatively large range, corresponding to a time to collision of about 30 s) and for the whole encounter duration, the angular rate estimates by the multi-sensor tracker enable a very accurate d_{CPA} estimation. On the

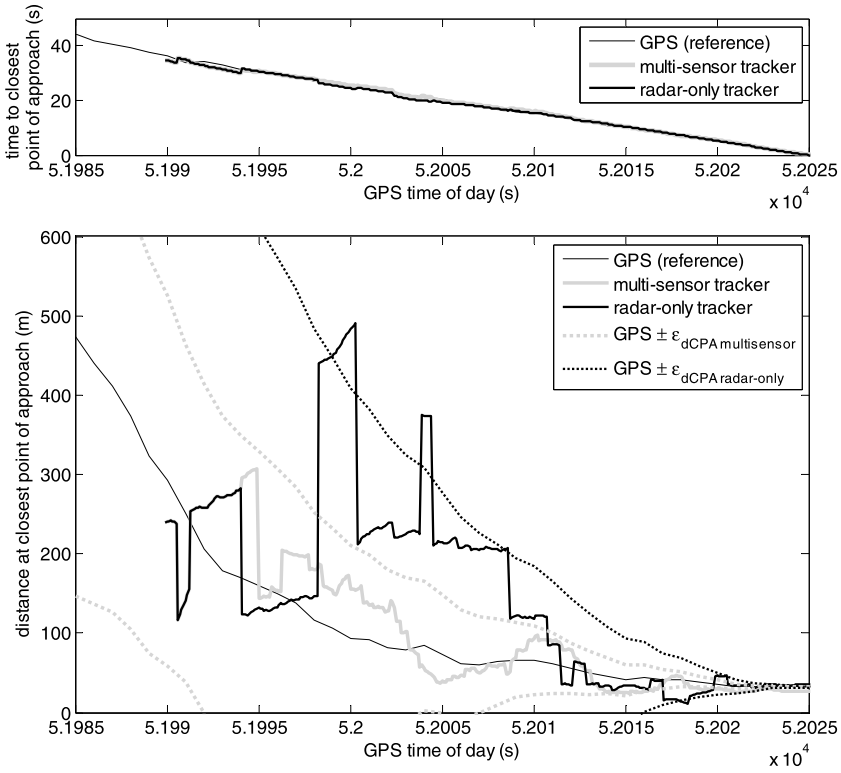

Fig. 15. Time to closest point of approach and distance at closest point of approach as a function of GPS time in the considered scenario.

other hand, while radar-based estimate is accurate at large range for some instants, its worse angular rate performance then leads to larger d_{CPA} error for more than 10 seconds, corresponding to a clearly worse collision detection performance. The phenomenon is mitigated only in the last seconds before closest point of approach, because the relatively small values of range and time to collision reduce the impact of angular rate errors.

Within the variability of experimental conditions, Fig. 15 shows that tracking outputs are very well contained in the envelopes defined by the uncertainty trends based on equations (5)–(7). While confirming the consistency of the simplified model, this further clarifies how the reduction by two thirds of the angular rate errors is the real key for improving accuracy in d_{CPA} estimation and thus collision detection performance. This conclusion holds in a general case: especially at large ranges, collision detection can be carried out with a satisfying trade-off between missed detection rates and false alarm rates by exploiting highly accurate angular rate estimates, which can only result from high resolution sensors, since these derivatives are indirectly estimated by the tracking algorithm.

5. Conclusions

This paper focused on algorithms and flight performance of radar/EO data fusion for non-cooperative UAS collision avoidance. Flight results were analyzed in detail and allow derivation of several lessons learned, beyond the aspects related to technology demonstration.

In spite of some experimental limitations, such as limited camera frame rate, data fusion is confirmed to provide a remarkable improvement of situational awareness compared with standalone radar tracking, while keeping the same reliability and avoiding false tracks and mis-association phenomena. In particular, while range and range rate performance is of the same order of magnitude of radar-based architectures, optimal integration of optical measurements enables a reduction by two thirds of error standard deviation in azimuth and elevation angles, attaining up to about 0.3°, and a similar reduction in the root mean square error in angular derivatives, up to about 0.1°/s. The change in angular rate performance corresponds to a significant accuracy improvement in the estimate of distance at closest point of approach, which is the basic variable used in collision detection logics. Indeed, larger frame rates would bring an even more significant performance increase, for the considered sensors. In general, both data rate and angular uncertainty of optical sensors are key factors to enhance tracking performance. In addition, increasing measurement rate is also important to ensure track continuity in case of intruder maneuvers, without needing a very conservative tuning of the tracking filter (large process noise) which would increase the risk of erroneous data association due to the generation of large track gating volumes.

Furthermore, though a multi-sensor architecture is more complex than a single sensor solution, flight experiments demonstrate that radar/EO fusion can be carried out with a relatively limited computational effort, and adopting commercial sensors and processing units.

Achieved results also confirm that data fusion effectiveness goes beyond the increase of tracking accuracy: exploitation of multi-sensor-based information within image processing algorithms for obstacle detection can significantly reduce false alarm rate, detection range sensitivity to weather and illumination conditions, and computational burden, which are all known issues of standalone EO systems. Thus, cross-sensor cueing represents a key factor to fully exploit the potential of multi-sensor architectures. Indeed, increasing detection range of optical sensors means reducing angular rate uncertainty at larger range (and time to collision) with a significant impact on collision detection performance because of the quadratic dependence of the uncertainty in estimated distance at closest point of approach on range in near collision geometries. Angular resolution is the main factor influencing detection range for given obstacle dimensions. Within this framework, multi-sensor architectures comprising cross-sensor cueing approaches provide a

convenient framework for integrating very high resolution/quantum efficiency cameras, also from the point of view of computational resources needed for monitoring a wide field of regard.

Obstacle detection sensors misalignment with respect to the AHRS-defined aircraft body reference frame, and biases in attitude measurement errors, do not have a significant impact on sense and avoid performance, which depends on the accuracy in predicting minimum separation in the future, more than on the instantaneous intruder position uncertainty. On the other hand, relative sensors alignment and accurate time registration represent key factors for fusion effectiveness.

Within multi-sensor systems aimed at an angular accuracy of the order of 0.1°, tracking performance depends on the ownship navigation unit even more than in single sensor architectures with coarse angular accuracy. First, attitude measurement error noise can worsen raw detection accuracy thus greatly reducing or even nullifying the advantage of integrating high resolution sensors. Then, instability of error biases can affect relative alignment accuracy if a flight-based procedure is implemented. Finally, regardless of sensors alignment, the same instability can affect angular rate performance by generating erroneous rate estimates, with consequent loss of data fusion advantage from the point of view of situational awareness. As an example, a fast change in heading error bias would result, at tracking level, in an erroneous azimuth rate estimate. Within this framework, it is interesting to underline that adoption of latest generation MEMS-based sensors has shown to be compatible with the above mentioned angular accuracy levels. This can be important in view of the adoption of data fusion approaches onboard UAS smaller than medium altitude long endurance (MALE) or high altitude long endurance (HALE) systems, which are usually equipped with tactical navigation units based on ring laser gyro technology. Miniaturization of airborne radar sensors could be a further driver in this direction.

Achieved results pave the way for two final considerations. On one hand, using current generation sensors, data fusion can fulfill safety requirements which would not be satisfied by single sensor architectures. More importantly, a multi-sensor-based approach can allow facing in a more effective and less expensive way the trade-offs relevant to design of new sensors for non-cooperative sense and avoid, since different sensors can be optimized in view of specific requirements

Conflict of interest statement

The authors declare that no conflict of interest exists.

Appendix A. Supplementary material

Supplementary material related to this article can be found online at http://dx.doi.org/10.1016/j.ast.2015.08.010.

References

[1] Association for Unmanned Vehicle Systems International (March 2013). The economic impact of Unmanned Aircraft Systems integration in the United States. [Online]. Available: http://www.auvsi.org/resources/economicreport.

[2] Federal Aviation Administration (November 2013). Integration of Civil Unmanned Aircraft Systems (UAS) in the National Airspace System (NAS) Roadmap, First Edition – 2013. [Online]. http://www.faa.gov/uas/legislative_programs/uas_roadmap/media/UAS_Roadmap_2013.pdf (accessed on 25 June 2015).

[3] Federal Aviation Administration. FAA Order 7610.4K, Ch. 12, Sec. 9-2, August 5, 2004.

[4] Federal Aviation Administration. Airworthiness certification of unmanned aircraft systems. FAA Order 8130.34, Washington, DC, March 27, 2008.

[5] EUROCONTROL, Specifications for the Use of Military Unmanned Aerial Vehicles as Operational Air Traffic Outside Segregated Airspace, version 1.0, 2007, doc. no. EUROCONTROL-SPEC-0102.

[6] A. Lacher, A. Zeitlin, D. Maroney, K. Markin, D. Ludwig, J. Boyd, Airspace integration alternatives for unmanned aircraft, in: AUVSI's Unmanned Systems Asia–Pacific 2010, Singapore, February 2010.

[7] K.R. Noth, Modeling and simulation of a ground based sense and avoid architecture for unmanned aircraft system operations, in: Integrated Communications, Navigation and Surveillance Conference (ICNS) 2011, Washington Dulles Airport, USA, 10–12 May 2011, pp. O7-1, O7-9.

[8] K. Foerster, M. Mullins, N. Kaabouch, W. Semke, Flight testing of a right-of-way compliant ADS-B-based miniature sense and avoid system, in: AIAA Infotech@Aerospace Conference 2012, Garden Grove, CA, 2012.

[9] P. Wehner, J. Schwartz, D. Hashemi, C.T. Howell III, H.A. Verstynen, C. Buttrill, M. Askelson, W. Semke, Evaluating prototype sense and avoid alternatives in simulation and flight, in: AUVSI – Unmanned Systems 2013, Washington, DC, August 2013.

[10] J. Utt, J. McCalmont, M. Deschenes, Development of a sense and avoid system, in: 1st AIAA Infotech@Aerospace Conference, Arlington, Virginia, September 26–29, 2005, pp. 1–10.

[11] J. Lai, J.J. Ford, L. Mejias, P. O'Shea, Characterization of sky-region morphological-temporal airborne collision detection, J. Field Robot. 30 (2) (March/April 2013) 171–193, http://dx.doi.org/10.1002/rob.21443.

[12] D. Dey, C.M. Geyer, S. Singh, M. Digioia, A cascaded method to detect aircraft in video imagery, Int. J. Robot. Res. 30 (12) (October 2011) 1527–1540.

[13] B. Vanek, T. Péni, A. Zarándyx, J. Bokor, T. Zsedrovits, T. Roska, Performance characteristics of a complete vision only sense and avoid system, in: AIAA Guidance, Navigation, and Control Conference, Minneapolis, MN, 13–16 August 2012, 2012.

[14] G. Fasano, D. Accardo, A. Moccia, C. Carbone, U. Ciniglio, F. Corraro, S. Luongo, Multi-sensor-based fully autonomous non-cooperative collision avoidance system for unmanned air vehicles, J. Aerosp. Comput. Inf. Commun. 5 (October 2008) 338–360, http://dx.doi.org/10.2514/1.35145.

[15] R.H. Chen, A. Gevorkian, A. Fung, W.Z. Chen, Multi-sensor data integration for autonomous sense and avoid, in: AIAA Infotech@Aerospace Technical Conference, St. Louis, Missouri, March 2011, 2011.

[16] M. Melega, S. Lazarus, M. Lone, A. Savvaris, Autonomous sense & avoid capabilities based on aircraft performances estimation, Proc. Inst. Mech. Eng., G J. Aerosp. Eng. 228 (4) (2014) 492–517.

[17] C. Le Tallec, VFR general aviation aircraft and UAV flights deconfliction, Aerosp. Sci. Technol. 9 (6) (September 2005) 495–503, http://dx.doi.org/10.1016/j.ast.2005.01.001.

[18] L.J. Scally, M. Bonato, Unmanned sense and avoid radar (USTAR), in: AIAA Infotech@Aerospace Technical Conference, St. Louis, Missouri, March 2011, 2011.

[19] S. Kemkemian, M. Nouvel-Fiani, P. Cornic, P. Garrec, A wide field of view radar for sense and avoid on UAV using space coloring waveforms, in: Proceedings of the 7th European Radar Conference, Paris, France, 30 September–1 October 2010, 978-2-87487-019-4.

[20] D. Accardo, G. Fasano, L. Forlenza, A. Moccia, A. Rispoli, Flight test of a radar-based tracking system for UAS sense and avoid, IEEE Trans. Aerosp. Electron. Syst. 49 (2) (April 2013) 1139–1160.

[21] L. Forlenza, G. Fasano, D. Accardo, A. Moccia, Flight performance analysis of an image processing algorithm for integrated sense-and-avoid systems, Int. J. Aerosp. Eng. 2012 (2012), http://dx.doi.org/10.1155/2012/542165, Article ID 542165.

[22] S. Luongo, V. Di Vito, G. Fasano, D. Accardo, L. Forlenza, A. Moccia, Automatic collision avoidance system: design, development and flight tests, in: IEEE/AIAA 30th Digital Avionics Systems Conference (DASC), Seattle, WA, 16–20 October 2011, pp. 5C1-1, 5C1-10.

[23] R.E. Collin, Antennas and Radiowave Propagation, McGraw-Hill, 1985.

[24] G. Euliss, A. Christiansen, R. Athale, Analysis of laser-ranging technology for sense and avoid operation of unmanned aircraft systems: the trade-off between resolution and power, in: Proc. of SPIE, vol. 6962, 2008, pp. 696208.1–696208.10.

[25] R. Sabatini, A. Gardi, M.A. Richardson, LIDAR obstacle warning and avoidance system for unmanned aircraft, Int. J. Mech. Ind. Sci. Eng. 8 (4) (April 2014) 62–73.

[26] O. Shakernia, W.-Z. Chen, V.M. Raska, Passive ranging for UAV sense and avoid applications, in: AIAA Infotech@Aerospace 2005, Arlington, VA, 26–29 September 2005.

[27] L.A. Klein, Sensor and Data Fusion – A Tool for Information Assessment and Decision Making, Spie Press, Bellingham, WA, USA, 2004.

[28] S.S. Blackman, R.F. Popoli, Design and Analysis of Modern Tracking Systems, Artech House, Norwood, MA, 1999.

[29] I. Arasaratnam, Simon Haykin, Cubature Kalman filters, IEEE Trans. Autom. Control 54 (6) (June 2009) 1254, 1269, http://dx.doi.org/10.1109/TAC.2009.2019800.

[30] N.E. Smith, R.G. Cobb, S.J. Pierce, V.M. Raska, Optimal collision avoidance trajectories for unmanned/remotely piloted aircraft, in: AIAA Guidance, Navigation, and Control (GNC) Conference, Boston, MA, August 19–22, 2013, 2013.

[31] R.A. Singer, R.G. Sea, K.B. Housewright, Derivation and evaluation of improved tracking filter for use in dense multitarget environments, IEEE Trans. Inf. Theory 20 (4) (July 1974) 423–432.
[32] S.S. Blackman, Multiple-Target Tracking with Radar Applications, Artech House, Dedham, MA, USA, 1986.
[33] G. Fasano, D. Accardo, L. Forlenza, A. Renga, G. Rufino, U. Tancredi, A. Moccia, Real-time hardware-in-the-loop laboratory testing for multisensor sense and avoid systems, Int. J. Aerosp. Eng. 2013 (2013), http://dx.doi.org/10.1155/2013/748751, Article ID 748751.
[34] Y. Bar-Shalom, Update with out-of-sequence measurements in tracking: exact solution, IEEE Trans. Aerosp. Electron. Syst. 38 (3) (2002).
[35] G. Fasano, D. Accardo, A. Moccia, A. Rispoli, An innovative procedure for calibration of strapdown electro-optical sensors onboard unmanned air vehicles, Sensors 10 (1) (2010) 639–654.
[36] E.D. Kaplan, C.J. Hegarty, Understanding GPS – Principles and Applications, 2nd ed., Artech House, Boston/London, 2006.
[37] M.D. Shuster, S.D. Oh, Three-axis attitude determination from vector observations, J. Guid. Control 4 (1) (January–February 1981) 70–77.